Open flux in Saturn's magnetosphere

Sarah V. Badman[a,b,c], Caitriona M. Jackman[d,e], Jonathan D. Nichols[b], John T. Clarke[f], Jean-Claude Gérard[g]

[a]*Institute of Space and Astronautical Science, Japan Aerospace Exploration Agency (JAXA), Yoshinodai 3-1-1, Chuo-ku, Sagamihara, Kanagawa, 252-5210, Japan*
[b]*Department of Physics and Astronomy, University of Leicester, University Road, Leicester, LE1 7RH, UK*
[c]*Department of Physics, Lancaster University, Bailrigg, Lancaster, LA1 4YB, UK*
[d]*Department of Physics and Astronomy, University College London, Gower Place, London, WC1E 6BT, UK.*
[e]*Department of Physics and Astronomy, University of Southampton, SO17 1BJ*
[f]*Center for Space Physics, Boston University, 725 Commonwealth Avenue, Boston, MA 02215, USA*
[g]*LPAP - Université de Liège, Sart Tilman - B5c, 17 Allé du 6 Aout, 4000 - LIEGE, Belgium*

Abstract

We characterise the interaction between the solar wind and Saturn's magnetosphere by evaluating the amount of 'open' magnetic flux connected to the solar wind. This is deduced from a large set of Hubble Space Telescope images of the ultraviolet aurora, using the poleward boundary of the main aurora as a proxy for the open-closed field line boundary in the ionosphere. The amount of open flux is found to be 10–50 GWb, with a mean of 35 GWb. The typical change in open flux between consecutive observations separated by 10–60 h is −5 or +7 GWb. These changes are a result of imbalance between open flux creation at the dayside magnetopause and its closure in the magnetotail. The 5 GWb typical decrease in open flux is consistent with in situ measurements of the flux transported following a reconnection event. Estimates of average, net reconnection rates are found to be typically a few

Email address: s.badman@lancaster.ac.uk (Sarah V. Badman)

tens of kV, with some extreme examples of unbalanced magnetopause or tail reconnection occurring at $\sim$ 300 kV. The range of values determined suggest that Saturn's magnetosphere does not generally achieve a steady state between flux opening at the magnetopause and flux closure in the magnetotail. The percentage of magnetic flux which is open in Saturn's magnetosphere is similar to that measured at the Earth (2–11%), but the typical percentage that is closed between observations is significantly lower (13% compared to 40–70%). Therefore, open flux is usually closed in smaller (few GWb) events in Saturn's magnetosphere. The exception to this behaviour is large, rapid flux closure events which are associated with solar wind compressions. While the rates of flux opening and closure should be equal over long timescales, they are evidently different on shorter (up to tens of hours) timescales. The relative independence of the magnetopause and tail reconnection rates can be attributed to the long loading timescales required to transport open field lines into the tail.

Keywords: Saturn, magnetosphere, Aurorae, Ultraviolet observations

1. Introduction

The interaction of the solar wind and interplanetary magnetic field (IMF) with a planetary magnetosphere is important for the transfer of plasma and momentum between the different environments. In the Dungey (1963) description of an 'open' magnetosphere, this interaction is driven by magnetic reconnection between the planetary and interplanetary fields when they have an anti-parallel component at the dayside magnetopause. The open field lines are then dragged anti-sunward by the solar wind flow to form long magne-

totail lobes. A simple schematic of the open magnetosphere is shown in Figure 1a. To complete the circulation of flux, reconnection occurs again in the tail and results in closed planetary field lines planetward of the reconnection site, which return to the dayside, and tailward, disconnected field lines. The disconnected field lines can take the form of a closed loop, a plasmoid, followed by the post-plasmoid plasma sheet (PPPS), which is produced by rapid reconnection of open field lines planetward of the plasmoid (Richardson et al., 1987). This scenario is illustrated in Figure 1d.

The ionospheric footprint of the open field lines forms the approximately circular polar cap, the size of which is modulated by the balance between opening of flux at the dayside magnetopause and closure in the magnetotail. The side and polar views of the polar cap (bounded by the open-closed field line boundary, OCB) are illustrated in Figure 1b and c. When unbalanced magnetopause (flux-opening) reconnection occurs, the open-closed boundary expands to lower latitudes to accommodate the new open flux. Conversely, when open flux is removed via unbalanced tail reconnection, the open-closed boundary contracts to higher latitudes. This is shown in Figure 1e and f.

Observations of Saturn's aurorae show that they generally form a 'main oval' ring of emission circling the poles although with considerable substructure imposed (Broadfoot et al., 1981; Clarke et al., 2005). These aurorae are associated with an upward-directed (from the ionosphere) field-aligned current which lies close to the boundary between open and closed magnetic field lines, driven by the flow shear between sub-corotating open and outer magnetosphere flux tubes, and the near-rigid corotating middle and inner magnetospheric flux tubes (Cowley et al., 2004; Badman et al., 2006; Bunce

et al., 2008). The darker area poleward of the main auroral oval maps to open field lines, and its size is determined by the balance between opening of flux at the dayside magnetopause and closure in the magnetotail, as described above. In this case, observations of Saturn's aurora can be used to estimate the amount of open flux in Saturn's magnetosphere, and deduce the balance between magnetopause and tail reconnection (Badman et al., 2005; Belenkaya et al., 2007).

While the conditions which control the rate and location of reconnection at Saturn's magnetopause have been debated (Scurry and Russell, 1991; Grocott et al., 2009; Lai et al., 2012; Masters et al., 2012), observations at the magnetopause have provided evidence of an open magnetopause required to sustain the open polar caps (Huddleston et al., 1997; McAndrews et al., 2008; Lai et al., 2012; Badman et al., 2013). Likewise, reconnection events have been identified in Saturn's magnetotail (Bunce et al., 2005; Jackman et al., 2007, 2008a; Hill et al., 2008). Jackman et al. (2011) performed a superposed epoch analysis of 34 plasmoids identified so far, and found evidence for a significant PPPS at Saturn, representing the closure of a significant amount (3 GWb) of open flux in a typical reconnection event in Saturn's tail.

In this study the open flux content of Saturn's magnetosphere is estimated using a large collection of images of the UV aurora, using the poleward edge of the auroral emission as a proxy for the open-closed field line boundary. Its variation and rate of change are also estimated and compared to values obtained from in situ measurements by Cassini, and global MHD simulations, in order to characterise the balance of magnetopause and tail reconnection over different timescales at Saturn.

2. Auroral Images

This study employs 108 images of Saturn's UV aurora obtained by the Space Telescope Imaging Spectrograph (STIS) and Advanced Camera for Surveys (ACS) instruments onboard the Hubble Space Telescope (HST) during 2000–2013. The data were reduced and projected onto a latitude-local time grid following the methods described by Grodent et al. (2003) and Grodent et al. (2005) for STIS images during 2000–2005, and Clarke et al. (2009) for ACS images from 2007 onward. The auroral morphology during each campaign has been detailed by Gérard et al. (2004) (1997–2001 campaigns), Clarke et al. (2005) and Grodent et al. (2005) (2004 campaign), Gérard et al. (2006) (2005 campaign), Clarke et al. (2009) (2007–8 campaigns) and Nichols et al. (in preparation) (2011–13 campaigns).

For each campaign, when successive images were obtained on the same HST orbit, i.e. within an observing interval of < 45 min, these have been combined to increase the signal to noise. Although the instrument sensitivities and data reduction methods varied between campaigns on different years, in this study we are concerned only with relative intensity between the bright auroral and dark polar cap regions for each image, rather than their absolute values, so such differences do not affect our results.

3. Determining the auroral boundary and open flux estimates

Following previous studies (Badman et al., 2005) the poleward boundary of the auroral emission is used as a proxy for the open-closed field line boundary. The region poleward of this is generally much darker than the main aurora, as expected in the open field line region. The poleward bound-

ary was identified at intervals of 10° longitude (ϕ) using a largely automated method. First, an automated procedure searched for the strongest positive gradient in intensity along each meridian from the pole. These points were checked by eye and any extreme outliers removed. At these locations and in regions of faint emission or where a strong gradient could not be identified, the boundary position was linearly interpolated between the values either side. Examples of the boundaries obtained from this method are shown by the red crosses on the images in Figures 2–3.

The boundary points obtained define the 'polar cap' area in Saturn's ionosphere threaded by open field lines. To calculate the amount of open flux, Φ, a model of Saturn's magnetic field (Burton et al., 2010) is integrated over the polar cap area, following the method detailed by Badman et al. (2005) and employing a flux function $F(r, \theta)$ (e.g. Cowley and Bunce (2003)):

$$\Phi = \Delta\phi \Sigma_{n=1}^{36} F(R(\theta_n), \theta_n), \tag{1}$$

where $\Delta\phi = 10°$ is the width of each longitudinal sector, θ_n is the co-latitude of the boundary in longitude sector n, and $R(\theta_n)$ is the radius of the surface containing the auroral emissions at that co-latitude, which matches the altitude to which each HST image was projected. This surface is an oblate spheroid about the spin axis, with an equatorial radius R_e and polar radius R_p, i.e.

$$R(\theta) = \frac{R_e}{(1 + \epsilon cos^2\theta)^{1/2}} \tag{2}$$

where

$$\epsilon = \frac{{R_e}^2}{R_p} - 1 \tag{3}$$

The auroral images were all projected to the peak UV emission altitude of 1100 km above the 1 bar reference spheroid (Gérard et al., 2009).

The flux contained within a circular polar cap region centred on Saturn's magnetic pole, calculated using this method, is shown as a function of circle radius in degrees co-latitude in Figure 4. The solid line shows the relationship for the southern hemisphere and the dashed line represents the northern hemisphere. The difference between the two is caused by the quadrupole component of Saturn's magnetic field which results in a stronger surface field strength in the north than the south at a given latitude (Burton et al., 2010). Figure 4b shows a reduced range of radius and flux values relevant to those discussed in this study.

The uncertainty in the open flux estimates can arise from uncertainties in the projection method (including the fact that the finite altitudinal extent of the auroral curtain is not accounted for), the boundary extrapolation in regions of dim aurora, and the underlying approximation of the open-closed boundary by the poleward boundary of the aurora. While the first of these is readily quantified e.g. by Grodent et al. (2005) to be $\sim$ 1–2° depending on the position relative to the sub-observer point, the others are less precise. For example, auroral emissions can be present on open field lines as a result of field-aligned currents and particle precipitation associated with ongoing reconnection at the dayside magnetopause (Bunce et al., 2005). These features have been observed in Saturn's aurora in both HST and Cassini observations (Gérard et al., 2004, 2005; Radioti et al., 2011; Badman et al., 2012). However, the area affected is generally a small fraction of the total open field region and, in the absence of sequential images or corresponding in situ mea-

surements, it is difficult to confirm whether such features are indeed occurring on open field lines. Furthermore, Cassini crossings of the high-latitude nightside have shown that the region of upward field-aligned current associated with the main auroral emission can be latitudinally displaced from the apparent open-closed boundary determined from the particle flux measurements (Talboys et al., 2011). This could lead to a systematic over-estimate of the open flux using our method based on auroral observations, but it obviously requires more detailed study to reconcile the observations made by different instruments and at different local times (c.f. Bunce et al. (2008)). In the absence of more comprehensive determination of the boundary location, we therefore use the consistent approximation of the poleward boundary of the UV emission to represent the open-closed boundary and include a reasonable uncertainty in the boundary location of 2° latitude in our open flux estimates to account for these combined uncertainties.

4. Results

4.1. Open flux distribution

The distribution of open flux values, Φ, estimated using the above method is plotted in Figure 5. The lower panel shows a histogram of the values across bins of width 10 GWb, while the upper panel shows each value and its error bar. The distribution of values in the y-direction on the upper panel is simply to space the values so each error bar can be seen. The distribution extends between 10–50 GWb, with two outliers at 9.7 GWb and 50.6 GWb. The minimum open flux value would be enclosed by a circular boundary, centered on Saturn's magnetic pole, with a radius of $\sim 7.5°$ in the southern hemisphere

and $\sim 7^\circ$) in the northern hemisphere (see Figure 4b). The maximum flux values correspond to circles of radii $\sim 17^\circ$ in the southern hemisphere and $\sim 15.5^\circ$) in the northern hemisphere, hence there is considerable variability in the size of Saturn's polar cap.

The median value of the open flux distribution is ~ 35 GWb, marked by the vertical dashed line on Figure 5. This amount of open flux would be contained by a circular boundary centred on Saturn's pole with radius $\sim 14^\circ$ in the southern hemisphere and $\sim 13^\circ$ in the northern hemisphere. The mean value is the same. The vertical dotted lines indicate the first and third quartiles of the distribution, which are 29.8 GWb and 42.0 GWb, respectively.

4.2. Sequences of open flux estimates

To investigate the time variability of the open flux content, the estimates for each sequence of images from 2004–2013 are plotted versus time in Figure 6a–f. The grey and black dots mark the open flux estimate for each image and the coloured shading gives the uncertainty range. The black dots in the 2007 and 2008 sequences highlight the estimates obtained from the images shown in Figures 2 and 3. The time distributions are referenced to the time of the minimum open flux value of each sequence, to facilitate comparison of open flux loading and unloading trends.

The distributions for all sequences are plotted together by the coloured lines in Figure 6g. We consider the decrease in open flux to the minimum of each sequence, for those where the minimum value was in the first quartile of the open flux distribution (< 30 GWb, from Figure 5). Two different trends are observed. The first is a steady decrease over ~ 5 days, as seen in the 2007

(cyan), 2011 (yellow), and 2012 (orange) sequences. Example auroral images used to estimate the open flux content over the interval in 2007 encompassing the minimum value are shown with the open flux boundaries in Figure 2. The open flux decreased from $\sim$ 40 GWb to $\sim$ 18 GWb (Figures 2a–g) in 2007, $\sim$ 33 GWb to $\sim$ 16 GWb in 2011, and $\sim$ 43 GWb to $\sim$ 26 GWb in 2012.

The second trend is a sharper decrease occurring over less than 2 days, as identified in the 2004 (black), 2008 (green), and 2013 (red) sequences, which is illustrated in Figure 3 for the 2008 sequence. The open flux content reduced from $\sim$ 32 GWb to $\sim$ 10 GWb in 2004, $\sim$ 35 GWb to $\sim$ 18 GWb (Figures 3a–b) in 2008, and $\sim$ 32 GWb to $\sim$ 24 GWb in 2013. The first of these was the largest decrease in open flux ($\sim$ 22 GWb) estimated from all pairs of consecutive images used in this study. These decreases are correlated with the occurrence of solar wind compressions at Saturn identified by Clarke et al. (2005, 2009); Badman et al. (2005); Belenkaya et al. (2008).

The 2005 sequence (dark blue) was unusual in showing very little variation in open flux (37–44 GWb) over its week-long duration. Gérard et al. (2006) noted that this campaign took place under particularly 'quiet' magnetospheric conditions.

The recovery from the minimum flux value also displays different behaviour between campaigns. The 2007 images indicate the most rapid subsequent increase in open flux content in this study, from $\sim$ 22 GWb to $\sim$ 39 GWb in $\sim$ 1 day (shown in Figures 2g–h). The 2004 (black) and 2008 (green) campaigns accumulate a similar amount of open flux in total but over 3–4 d. The latter is shown in Figure 3b–e.

4.3. Changes in open flux

To investigate the typical change in open flux content, pairs of successive images spaced by $10 < \Delta t < 60$ h were selected. This resulted in 61 pairs of images. The lower time limit is imposed because evaluating changes in open flux with their implicit uncertainties over short timescales of a few hours or less can lead to excessively high estimated reconnection rates. The validity of this limit is also affirmed by the study by Jackman et al. (2011), who detected multiple magnetic field signatures of plasmoids in Saturn's magnetotail during an interval of ~ 3 h. These could be counted together as a single flux closure event. The upper limit of 60 h corresponds to the expected occurrence interval between tail reconnection events involving unloading of open flux, as found in the same study. Changes in flux over longer time intervals are more likely to be attributed to multiple, separate reconnection events, which would become indistinguishable if a longer time interval were used. Furthermore, we are interested in determining the changes in open flux observed, which would tend to average to zero over increasingly long timescales.

The changes in open flux, $\Delta\Phi$, estimated between two consecutive images are plotted against the time interval between the images, Δt, in Figure 7a. The error bars account for the uncertainty in the open flux estimates. It is clear that a wide range of both positive (net flux opening) and negative (net flux closure) changes in open flux content were observed over all the time intervals considered. This indicates that the open flux content of Saturn's magnetosphere is far from steady.

The occurrence distribution of $\Delta\Phi$ is plotted in Figure 7b. The grey

shaded distribution represents all the values estimated while the solid line represents the distribution of only those values of $\Delta\Phi$ larger than their associated errors (43 values in total). The vertical dashed lines show the median positive and negative values for the reduced distribution. These distributions show that most of the net changes in open flux observed, $\Delta\Phi$, were less than ± 5 GWb over the time intervals studied, but that approximately half of these were small compared to their associated uncertainty. The median increases and decreases in open flux for the reduced distribution (where $\Delta\Phi$ is larger than its uncertainty) were $+7$ GWb and -5 GWb. However, the maximum changes observed were larger than 20 GWb.

These estimates of decreases in open flux are in good agreement with estimates of the amount of newly-closed flux transported in the PPPS made by Jackman et al. (2011): up to ~ 6 GWb in a 3 h case study of multiple plasmoid encounters, and an average of up to ~ 3 GWb per event for all observations made.

4.4. Average, net reconnection rates

The time over which these changes in open flux was observed must also be considered. To do this, the average, net reconnection rate was calculated for each pair of images using $V_{avg,net} = \Delta\Phi/\Delta t$. Of course this cannot distinguish the separate rates of flux opening and closure, but while the rates must be equal over long timescales, they may be different over shorter intervals of time, such as those considered here.

The distribution of the derived $V_{avg,net}$ values are plotted in bins of 50 kV width in Figure 7c. As in panel (b), the grey shaded distribution represents all the values estimated while the solid line represents the reduced distribu-

tion. The majority of the values are clustered between ±100 kV but half of these are not significant compared to their errors. The median positive and negative $V_{avg,net}$ values of the reduced distribution are +80 kV and −60 kV. The overall mean is 3 kV, i.e. close to zero, confirming that the flux opening and closing rates are equal over a long time interval.

The median positive flux loading rate is similar to the average and spot values derived for flux opening at the magnetopause in previous studies (Jackman et al., 2004; Badman et al., 2005; McAndrews et al., 2008; Radioti et al., 2011). These values correspond to intermediate driving by the solar wind, based on empirical estimates of magnetopause reconnection rates by Jackman et al. (2004), while the maximum value, up to 305 kV, corresponds to strong driving in a solar wind compression region.

4.5. Conditioning

We next consider whether there is any dependence of the net reconnection rate on the initial or final amount of open flux present for those cases where the changes in flux are larger than the associated uncertainties. Figure 8a shows the distribution of average, net reconnection rates, $V_{avg,net}$ versus the initial amount of open flux, Φ_1, estimated from the first of the two consecutive images. Similarly, Figure 8b shows the distribution of $V_{avg,net}$ versus the final amount of open flux, Φ_2, estimated from the second of the two consecutive images. The distributions in the lower panels, c and d, of Figure 8 show the relative occurrence of the positive (upper, dark grey shading) and negative (lower, light grey) values of $V_{avg,net}$ in each 10 GWb open flux bin.

The relative heights of the bars in Figure 8c show that larger values of open flux tend to be followed by negative net reconnection rates, i.e. large

open flux content tends to decrease. If the initial amount of open flux was above 30 GWb, negative net reconnection rates were more often deduced to follow, while if the starting amount of open flux was lower than 30 GWb, positive reconnection rates were more often deduced (smaller open fluxes tended to increase).

When comparing the net reconnection rates to their 'final' open flux values, Φ_2, shown in Figure 8b and d, a trend in the opposite sense is observed. Low open fluxes of < 30 GWb were three times more likely to be observed after intervals of net flux closure. Net positive reconnection rates were more frequently deduced preceding larger (> 40 GWb) open flux values.

While these trends seem intuitive, the fact that they are evident in a large selection of images reveals that the reconnection rates are usually significantly unbalanced over the various timescales considered in this study (10–60 h). That is, Saturn's magnetosphere does not generally display a balanced 'steady-state' of solar wind interaction.

A final way to quantify this trend is to estimate the average and maximum amount of open flux closed as a fraction of the initial open flux, i.e. $\Delta\Phi/\Phi_1$. The maximum is found to be 69%, and the median (mean) across all pairs of images is 13(18)%. The significance of these values will be discussed more below.

5. Discussion

In the previous sections the averages and extrema of the open flux content of Saturn's magnetosphere, and their net rates of change, have been deduced. Next, these values will be interpreted in comparison with estimates for the

Earth and Mercury, and their implications for the magnetospheric interaction with the solar wind will be discussed. In this study, as described in the Introduction, magnetic flux opening is considered to occur at the dayside magnetopause, wherever the magnetic fields have an anti-parallel component, while flux closure is generally considered to occur in the magnetotail. The closure of magnetic flux at the dayside magnetopause via dual lobe reconnection under southward IMF is not expected to be significant at Saturn due to the predominantly azimuthal orientation of the IMF (Cowley et al., 2008; Jackman et al., 2008b).

There is no routine upstream monitoring of the IMF at Saturn such that we cannot comprehensively assess the IMF dependence of the open flux estimates obtained. IMF measurements were made by the Cassini spacecraft during a few auroral imaging sequences, most notably the January 2004 campaign (Clarke et al., 2005). During these intervals the estimates of open flux deduced from auroral images have been related to the IMF magnitude, direction, and the solar wind dynamic pressure (Badman et al., 2005; Belenkaya et al., 2007, 2008, 2010). These studies found that the open flux increased with increasing northward IMF (more positive B_Z) and decreased with increasing southward IMF (more negative B_Z). The reduction in open flux under southward IMF was less when a strong B_Y component was also present. The amount of open flux decreased following increases in solar wind dynamic pressure. We expect the same general dependences to occur for all the imaging sequences. However, the description in the following sections of the increases and decreases in open flux is based only on the observed changes in polar cap size, and is not conditional on assuming a certain prevalent IMF

orientation.

5.1. Open flux content

The amount of open flux in Saturn's magnetosphere has been estimated to be between 10 and 50 GWb, corresponding to 2–11% of the total magnetic flux in one hemisphere. This is essentially the same as the proportion of magnetic flux that has been identified by Milan et al. (2004) as open in the Earth's magnetosphere: 2.5–12%. At Mercury the estimated range is rather higher, with $\sim 30\%$ of the planetary flux contained in an open magnetotail during moderate loading events, and the suggestion that the magnetosphere could approach 100% open under extreme loading conditions (Slavin et al., 2010). Comparison of these values suggests that Saturn and the Earth have a similar average interaction with the solar wind and IMF, leading to similar open flux content, while Mercury's magnetosphere is generally more open.

Jia et al. (2012) performed a global MHD simulation of Saturn's magnetosphere under time-varying solar wind conditions. They found that the amount of open flux varied between ~ 20 and ~ 35 GWb under northward or azimuthal IMF conditions (implying anti-parallel or component reconnection at the dayside magnetopause). These values are below the average estimated from the auroral images in this study. The range of the values is also rather smaller than estimated from the images (10–50 GWb). The reason for these differences is not obvious and, as the reconnection rates in MHD simulations depend strongly on numerical diffusion in the code, we do not attempt to draw detailed conclusions on this.

The net amount of open flux closed over intervals between successive images was found to be ~ 5 GWb, which agrees well with estimates made

from in situ magnetometer data (Jackman et al., 2011). Similar estimates of the flux closed in tail reconnection events have also been obtained by a global MHD simulation of Saturn's magnetosphere by Jia et al. (2012), who found a range of 1–10 GWb, with a mean of 3.5 GWb. Expressing the amount of flux closed as a percentage of open flux originally present yields a median (mean) value of $\sim$ 13(18)% per interval, with a maximum of $\sim$ 69%. In only 2 of 25 cases was the net flux closed greater than 40% of the open flux originally present.

This is in contrast to observations of the Earth's magnetotail, where typically 40–70% of the open flux in the magnetotail is closed in a substorm (flux closure event), and these large reconnection bursts provide the major or only source of flux closure (Milan et al., 2003, 2007). It seems, therefore, that while the average amount of planetary flux connected to the solar wind is the same for the Earth and Saturn, the processes leading to open flux loading and unloading may be quite different. Small amounts of open flux could frequently be closed in post-plasmoid lobe reconnection events, such as those described by Jackman et al. (2011), while the large-scale compressions of the magnetosphere associated with solar wind shocks result in less-frequent, large flux closure events, more like terrestrial substorms, and may be induced by increased magnetic pressure in the compressed magnetotail (e.g. Badman et al., 2005; Jia et al., 2012). It is important to remember that only the net changes in open flux are deduced in this study and the amounts of open flux loading and unloading in each interval cannot be separated without an upstream solar wind monitor. If, however, the open flux is usually removed via small closure events, the open flux loading events should similarly be small

or occurring over long timescales.

5.2. Reconnection rates

In the absence of simultaneous in situ measurements of the separate tail and magnetopause reconnection rates, we have been able to deduce only the net change in open flux from the auroral images. It is likely that the reconnection rates in the tail or at the magnetopause will sometimes be significantly higher than the values obtained in this study but proceeding in both locations at the same time, as identified in the Earth's magnetosphere e.g. by Milan et al. (2007). Furthermore these are average values determined over 10–60 h intervals, while the reconnection rates may be significantly higher but lasting for correspondingly shorter intervals. These differences have been estimated and discussed by Badman et al. (2005) for the 2004 dataset when Cassini was measuring the IMF upstream of Saturn.

The present analysis suggests that open flux is usually added to Saturn's polar cap at an average rate of a few tens of kV. Stronger loading events, with average flux transfer greater than 200 kV are deduced in only one case. Flux closure events usually proceed at a similar average rate of a few tens of kV, with a single, maximum net flux transfer rate of 275 kV.

Despite the uncertainties described above, the values determined in this study are in agreement with previous estimates of magnetopause reconnection voltages. For example, Jackman et al. (2004) used an empirical algorithm scaled from studies at the Earth to estimate the rate of flux opening at Saturn's magnetopause. They found average reconnection rates of between $\sim$ 10 kV and $\sim$ 400 kV in rarefied and compressed solar wind conditions, respectively. McAndrews et al. (2008) estimated the reconnection voltage

from magnetic field and plasma data acquired during a crossing of the magnetopause by Cassini, and found an intermediate value of 48 kV.

Furthermore, because of the long timescales for transport of newly-opened flux tubes from the dayside magnetopause to the magnetotail lobes (few days, (Jackman et al., 2004)), the tail dynamics and possible terrestrial substorm-like activity (i.e. flux closure events) are not expected to respond immediately to dayside driving, therefore it is reasonable to expect that magnetopause and tail reconnection can proceed independently of each other. We therefore conclude that our net voltage estimates are representative of the average magnetopause and tail reconnection rates which occurred. Overall, the fact that a wide range of both positive and negative net reconnection rates have been derived, including some particularly large values, suggests that Saturn's magnetosphere does not achieve a steady interaction with the solar wind over the timescales considered.

6. Conclusions

The open flux content of Saturn's magnetosphere has been estimated based on a large set of auroral images, and found to lie within 10–50 GWb, with a mean of 35 GWb. These values, and their variability are considerably higher than those determined from global simulations of Saturn's magnetosphere e.g. Jia et al. (2012).

Estimates of average, net reconnection rates have also been made by comparing open flux estimates separated by intervals of 10–60 h, and are found to be typically a few tens of kV, with some extreme examples of unbalanced magnetopause or tail reconnection occurring at up to 270 kV. The average

increase in open flux between images was 7 GWb and the average decrease was 5 GWb. The largest open fluxes ($>$ 40 GWb) tended to decrease by 2–7 GWb. The smallest open fluxes ($<$ 30 GWb) usually followed decreases of 6–20 GWb. The range of values determined suggest that Saturn's magnetosphere does not generally achieve a balance between flux opening at the magnetopause and flux closure in the magnetotail.

A further clue to this behaviour is that while the amount of open flux at Saturn is similar to that measured at the Earth (2–11%), the typical fraction that is closed over the intervals studied is significantly lower (13% compared to 40–70%). Therefore, open flux is usually closed in smaller (few GWb) events in Saturn's magnetosphere. The exception to this behaviour is the large, rapid flux closure events which are associated with solar wind compressions, as identified in the 2004 data set by Badman et al. (2005). While the rates of flux opening and closure should be equal over long timescales, they are evidently different on shorter (up to tens of hours) timescales. The independence of the magnetopause and tail reconnection rates, compared to those observed at the Earth can be attributed to the long loading timescales required to transport open field into the tail.

These results provide useful constraints for models of magnetospheric dynamics and the extent of the interaction with the solar wind, and for diagnosing the time history of magnetospheric dynamics from remote auroral observations.

Acknowledgments SVB was supported by a JAXA Research Fellowship and a Royal Astronomical Society Research Fellowship. CMJ was supported by a Leverhulme Trust Early Career Fellowship. This work is based on

observations with the NASA/ESA Hubble Space Telescope obtained at the Space Telescope Science Institute (STScI), which is operated by AURA, inc. for NASA. This research was partly supported by the PRODEX Program managed by the European Space Agency in collaboration with the Belgian Federal Science Policy Office.

References

Badman, S.V., Achilleos, N., Arridge, C.S., Baines, K.H., Brown, R.H., Bunce, E.J., Coates, A.J., Cowley, S.W.H., Dougherty, M.K., Fujimoto, M., Hospodarsky, G., Kasahara, S., Kimura, T., Melin, H., Mitchell, D.G., Stallard, T., Tao, C., 2012. Cassini observations of ion and electron beams at Saturn and their relationship to infrared auroral arcs. J. Geophys. Res. 117.

Badman, S.V., Bunce, E.J., Clarke, J.T., Cowley, S.W.H., Gérard, J.C., Grodent, D., Milan, S.E., 2005. Open flux estimates in Saturn's magnetosphere during the January 2004 Cassini-HST campaign, and implications for reconnection rates. J. Geophys. Res. 110.

Badman, S.V., Cowley, S.W.H., Gérard, J.C., Grodent, D., 2006. A statistical analysis of the location and width of Saturn's southern auroras. Ann. Geophys. 24, 3533–3545.

Badman, S.V., Masters, A., Hasegawa, H., Fujimoto, M., Radioti, A., Grodent, D., Sergis, N., Dougherty, M.K., Coates, A.J., 2013. Bursty magnetic reconnection at Saturn's magnetopause. Geophys. Res. Lett. 40, 1027–1031.

489 Belenkaya, E.S., Alexeev, I.I., Blokhina, M.S., Bunce, E.J., Cowley, S.W.H.,
490 Nichols, J.D., Kalegaev, V.V., Petrov, V.G., Provan, G., 2010. IMF de-
491 pendence of Saturn's auroras: modelling study of HST and Cassini data
492 from 12-15 February 2008. Ann. Geophys. 28, 1559–1570.

493 Belenkaya, E.S., Alexeev, I.I., Blokhina, M.S., Cowley, S.W.H., Badman,
494 S.V., Kalegaev, V.V., Grigoryan, M.S., 2007. IMF dependence of the open-
495 closed field line boundary in Saturn's ionosphere, and its relation to the
496 UV auroral oval observed by the Hubble Space Telescope. Ann. Geophys.
497 25, 1215–1226.

498 Belenkaya, E.S., Cowley, S.W.H., Badman, S.V., Blokhina, M.S., Kalegaev,
499 V.V., 2008. Dependence of the open-closed field line boundary in Saturn's
500 ionosphere on both the IMF and solar wind dynamic pressure: comparison
501 with the UV auroral oval observed by the HST. Ann. Geophys. 26, 159–
502 166.

503 Broadfoot, A.L., Sandel, B.R., Shemansky, D.E., Holberg, J.B., Smith, G.R.,
504 Strobel, D.F., McConnell, J.C., Kumar, S., Hunten, D.M., Atreya, S.K.,
505 Donahue, T.M., Moos, H.W., Bertaux, J.L., Blamont, J.E., Pomphrey,
506 R.B., Linick, S., 1981. Extreme ultraviolet observations from Voyager-1
507 encounter with Saturn. Science 212, 206–211.

508 Bunce, E.J., Arridge, C.S., Clarke, J.T., Coates, A.J., Cowley, S.W.H.,
509 Dougherty, M.K., Gérard, J.C., Grodent, D., Hansen, K.C., Nichols, J.D.,
510 Southwood, D.J., Talboys, D.L., 2008. Origin of Saturn's aurora: Simul-
511 taneous observations by Cassini and the Hubble Space Telescope. J. Geo-
512 phys. Res. 113.

513 Bunce, E.J., Cowley, S.W.H., Milan, S.E., 2005. Interplanetary magnetic
514 field control of Saturn's polar cusp aurora. Ann. Geophys. 23, 1405–1431.

515 Burton, M.E., Dougherty, M.K., Russell, C.T., 2010. Saturn's internal plan-
516 etary magnetic field. Geophys. Res. Lett. 37.

517 Clarke, J.T., Gérard, J.C., Grodent, D., Wannawichian, S., Gustin, J., Con-
518 nerney, J., Crary, F., Dougherty, M., Kurth, W., Cowley, S.W.H., Bunce,
519 E.J., Hill, T., Kim, J., 2005. Morphological differences between Saturn's
520 ultraviolet aurorae and those of Earth and Jupiter. Nature 433, 717–719.

521 Clarke, J.T., Nichols, J., Gerard, J.C., Grodent, D., Hansen, K.C., Kurth,
522 W., Gladstone, G.R., Duval, J., Wannawichian, S., Bunce, E., Cowley,
523 S.W.H., Crary, F., Dougherty, M., Lamy, L., Mitchell, D., Pryor, W.,
524 Retherford, K., Stallard, T., Zieger, B., Zarka, P., Cecconi, B., 2009. Re-
525 sponse of Jupiter's and Saturn's auroral activity to the solar wind. J. Geo-
526 phys. Res. 114.

527 Cowley, S.W.H., Badman, S.V., Imber, S.M., Milan, S.E., 2008. Comment
528 on "Jupiter: A fundamentally different magnetospheric interaction with
529 the solar wind" by D. J. McComas and F. Bagenal. Geophys. Res. Lett.
530 35.

531 Cowley, S.W.H., Bunce, E.J., 2003. Corotation-driven magnetosphere-
532 ionosphere coupling currents in Saturn's magnetosphere and their relation
533 to the auroras. Ann. Geophys. 21, 1691–1707.

534 Cowley, S.W.H., Bunce, E.J., O'Rourke, J.M., 2004. A simple quantitative

535 model of plasma flows and currents in Saturn's polar ionosphere. J. Geo-
536 phys. Res. 109.

537 Dungey, J.W., 1963. The structure of the exosphere or adventures in velocity
538 space, in: De Witt, C., Hieblot, J., Le Beau, L. (Eds.), Geophysics, The
539 Earth's Environment, p. 503.

540 Gérard, J.C., Bonfond, B., Gustin, J., Grodent, D., Clarke, J.T., Bisikalo,
541 D., Shematovich, V., 2009. Altitude of Saturn's aurora and its implications
542 for the characteristic energy of precipitated electrons. Geophys. Res. Lett.
543 36.

544 Gérard, J.C., Bunce, E.J., Grodent, D., Cowley, S.W.H., Clarke, J.T., Bad-
545 man, S.V., 2005. Signature of Saturn's auroral cusp: Simultaneous Hubble
546 Space Telescope FUV observations and upstream solar wind monitoring.
547 J. Geophys. Res. 110.

548 Gérard, J.C., Grodent, D., Cowley, S.W.H., Mitchell, D.G., Kurth, W.S.,
549 Clarke, J.T., Bunce, E.J., Nichols, J.D., Dougherty, M.K., Crary, F.J.,
550 Coates, A.J., 2006. Saturn's auroral morphology and activity during quiet
551 magnetospheric conditions. J. Geophys. Res. 111.

552 Gérard, J.C., Grodent, D., Gustin, J., Saglam, A., Clarke, J.T., Trauger,
553 J.T., 2004. Characteristics of Saturn's FUV aurora observed with the
554 Space Telescope Imaging Spectrograph. J. Geophys. Res. 109.

555 Grocott, A., Badman, S.V., Cowley, S.W.H., Milan, S.E., Nichols, J.D.,
556 Yeoman, T.K., 2009. Magnetosonic Mach number dependence of the ef-

ficiency of reconnection between planetary and interplanetary magnetic fields. J. Geophys. Res. 114.

Grodent, D., Clarke, J.T., Kim, J., Waite, J.H., Cowley, S.W.H., 2003. Jupiter's main auroral oval observed with HST-STIS. J. Geophys. Res. 108, 1389.

Grodent, D., Gérard, J.C., Cowley, S.W.H., Bunce, E.J., Clarke, J.T., 2005. Variable morphology of Saturn's southern ultraviolet aurora. J. Geophys. Res. 110.

Hill, T.W., Thomsen, M.F., Henderson, M.G., Tokar, R.L., Coates, A.J., McAndrews, H.J., Lewis, G.R., Mitchell, D.G., Jackman, C.M., Russell, C.T., Dougherty, M.K., Crary, F.J., Young, D.T., 2008. Plasmoids in Saturn's magnetotail. J. Geophys. Res. 113.

Huddleston, D.E., Russell, C.T., Le, G., Szabo, A., 1997. Magnetopause structure and the role of reconnection at the outer planets. J. Geophys. Res. 102, 24289–24302.

Jackman, C.M., Achilleos, N., Bunce, E.J., Cowley, S.W.H., Dougherty, M.K., Jones, G.H., Milan, S.E., Smith, E.J., 2004. Interplanetary magnetic field at ∼9 AU during the declining phase of the solar cycle and its implications for Saturn's magnetospheric dynamics. J. Geophys. Res. 109.

Jackman, C.M., Arridge, C.S., Krupp, N., Bunce, E.J., Mitchell, D.G., McAndrews, H.J., Dougherty, M.K., Russell, C.T., Achilleos, N., Jones, G.H., Coates, A.J., 2008a. A multi-instrument view of tail reconnection at Saturn. J. Geophys. Res. 113.

580 Jackman, C.M., Forsyth, R.J., Dougherty, M.K., 2008b. The overall configu-
581 ration of the interplanetary magnetic field upstream of Saturn as revealed
582 by Cassini observations. J. Geophys. Res. 113.

583 Jackman, C.M., Russell, C.T., Southwood, D.J., Arridge, C.S., Achilleos, N.,
584 Dougherty, M.K., 2007. Strong rapid dipolarizations in Saturn's magne-
585 totail: In situ evidence of reconnection. Geophys. Res. Lett. 34.

586 Jackman, C.M., Slavin, J.A., Cowley, S.W.H., 2011. Cassini observations of
587 plasmoid structure and dynamics: Implications for the role of magnetic
588 reconnection in magnetospheric circulation at Saturn. J. Geophys. Res.
589 116.

590 Jia, X., Hansen, K.C., Gombosi, T.I., Kivelson, M.G., Tóth, G., DeZeeuw,
591 D.L., Ridley, A.J., 2012. Magnetospheric configuration and dynamics of
592 Saturn's magnetosphere: A global MHD simulation. J. Geophys. Res. 117.

593 Lai, H.R., Wei, H.Y., Russell, C.T., Arridge, C.S., Dougherty, M.K., 2012.
594 Reconnection at the magnetopause of Saturn: Perspective from FTE oc-
595 currence and magnetosphere size. J. Geophys. Res. 117.

596 Masters, A., Eastwood, J.P., Swisdak, M., Thomsen, M.F., Russell, C.T.,
597 Sergis, N., Crary, F.J., Dougherty, M.K., Coates, A.J., Krimigis, S.M.,
598 2012. The importance of plasma β conditions for magnetic reconnection
599 at Saturn's magnetopause. Geophys. Res. Lett. 39.

600 McAndrews, H.J., Owen, C.J., Thomsen, M.F., Lavraud, B., Coates, A.J.,
601 Dougherty, M.K., Young, D.T., 2008. Evidence for reconnection at Sat-
602 urn's magnetopause. J. Geophys. Res. 113.

Milan, S.E., Cowley, S.W.H., Lester, M., Wright, D.M., Slavin, J.A., Fillingim, M., Carlson, C.W., Singer, H.J., 2004. Response of the magnetotail to changes in the open flux content of the magnetosphere. J. Geophys. Res. 109.

Milan, S.E., Lester, M., Cowley, S.W.H., Oksavik, K., Brittnacher, M., Greenwald, R.A., Sofko, G., Villain, J.P., 2003. Variations in the polar cap area during two substorm cycles. Ann. Geophys. 21, 1121–1140.

Milan, S.E., Provan, G., Hubert, B., 2007. Magnetic flux transport in the Dungey cycle: A survey of dayside and nightside reconnection rates. J. Geophys. Res. 112.

Radioti, A., Grodent, D., Gérard, J.C., Milan, S.E., Bonfond, B., Gustin, J., Pryor, W.R., 2011. Bifurcations of the main auroral ring at Saturn: ionospheric signatures of consecutive reconnection events at the magnetopause. J. Geophys. Res. 116.

Richardson, I.G., Cowley, S.W.H., Hones, Jr., E.W., Bame, S.J., 1987. Plasmoid-associated energetic ion bursts in the deep geomagnetic tail - Properties of plasmoids and the postplasmoid plasma sheet. J. Geophys. Res. 92, 9997–10013.

Scurry, L., Russell, C.T., 1991. Proxy studies of energy transfer to the magnetosphere. J. Geophys. Res. 96, 9541–9548.

Slavin, J.A., Anderson, B.J., Baker, D.N., Benna, M., Boardsen, S.A., Gloeckler, G., Gold, R.E., Ho, G.C., Korth, H., Krimigis, S.M., McNutt, R.L., Nittler, L.R., Raines, J.M., Sarantos, M., Schriver, D., Solomon,

626 S.C., Starr, R.D., Trávníček, P.M., Zurbuchen, T.H., 2010. MESSENGER
627 Observations of Extreme Loading and Unloading of Mercury's Magnetic
628 Tail. Science 329, 665–668.

629 Talboys, D.L., Bunce, E.J., Cowley, S.W.H., Arridge, C.S., Coates, A.J.,
630 Dougherty, M.K., 2011. Statistical characteristics of field-aligned currents
631 in Saturn's nightside magnetosphere. J. Geophys. Res. 116.

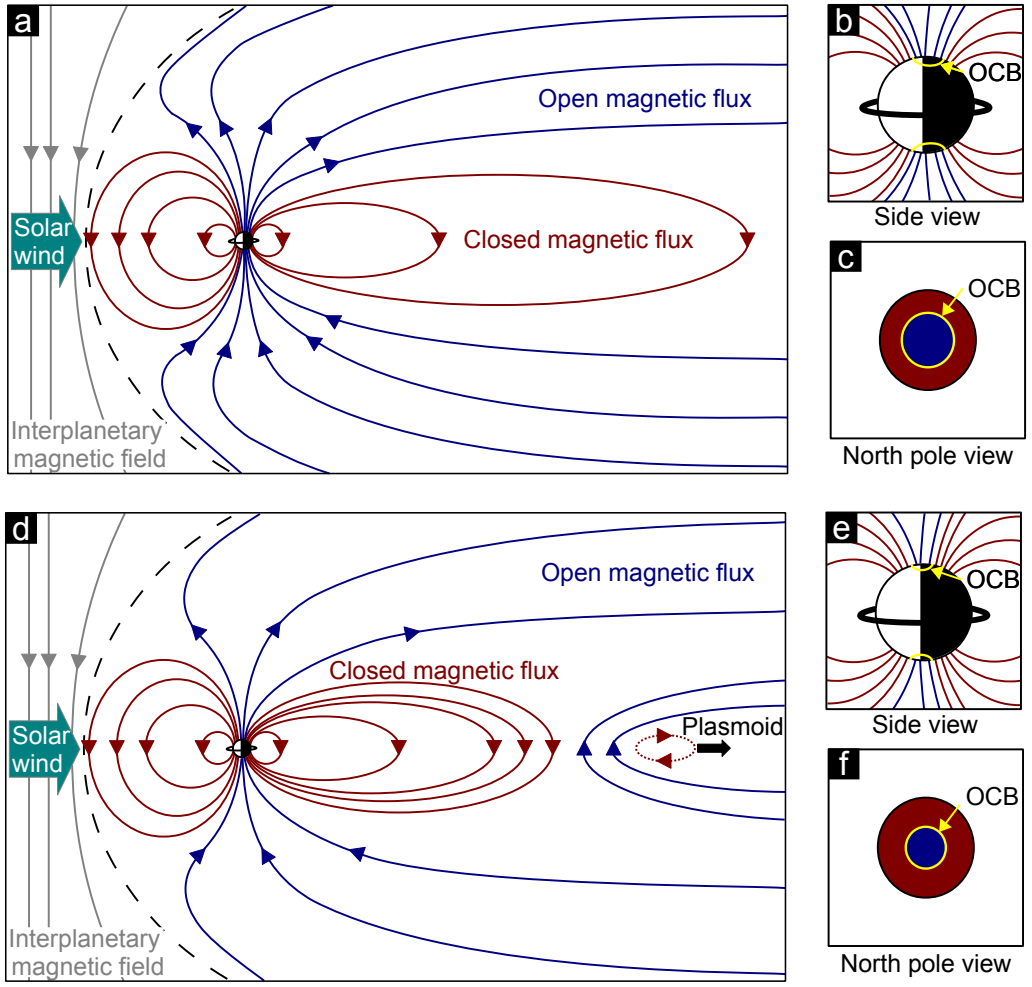

Figure 1: Schematic of Saturn's open magnetosphere (a) before, and (d) after a tail reconnection event which closes some of the open flux in the tail lobes. (b) and (e) The corresponding locations of the open-closed field line boundary (OCB) in the ionosphere. (c) and (f) The polar view of the OCB.

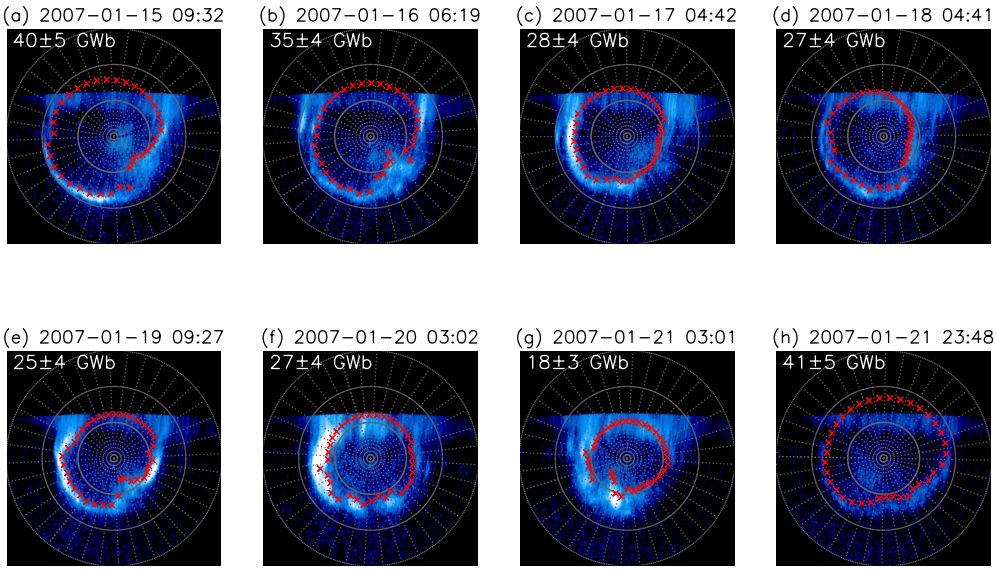

Figure 2: Sequence of images of the southern UV aurorae from the 2007 campaign. The images are polar projected with local noon to the bottom and dawn to the left. A portion of the nightside of each image is cut off where the viewing angle was 90° and higher because of uncertainties in the projection beyond this limit. The grey grid marks 10° lines of longitude and latitude. The start time of each image is labelled at the top. The red crosses mark the estimated boundary of the open flux region. The open flux estimate is labelled in the top left corner of each panel.

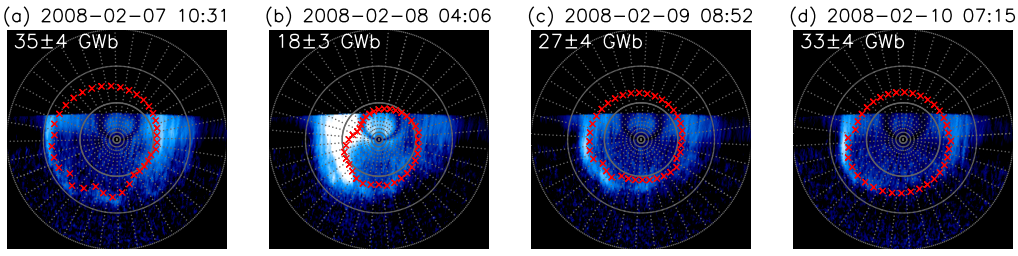

Figure 3: Sequence of images of the southern UV aurorae from the 2008 campaign in the same format as Figure 2.

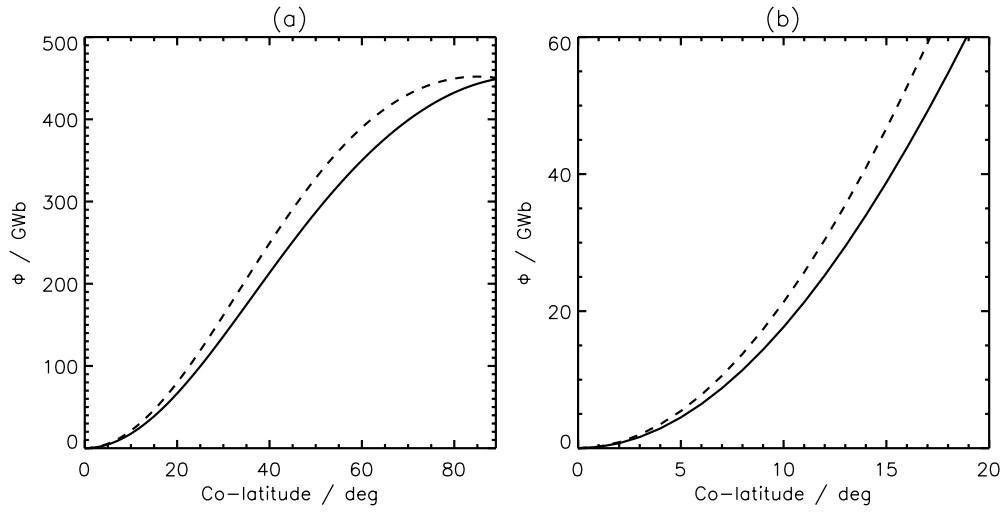

Figure 4: Magnetic flux, Φ, enclosed by a circular boundary centred on Saturn's magnetic pole as a function of co-latitudinal radius. The solid line represents the southern hemisphere and the dashed line represents the northern hemisphere. (a) The full co-latitude range. (b) A reduced range pertinent to the values discussed in this study.

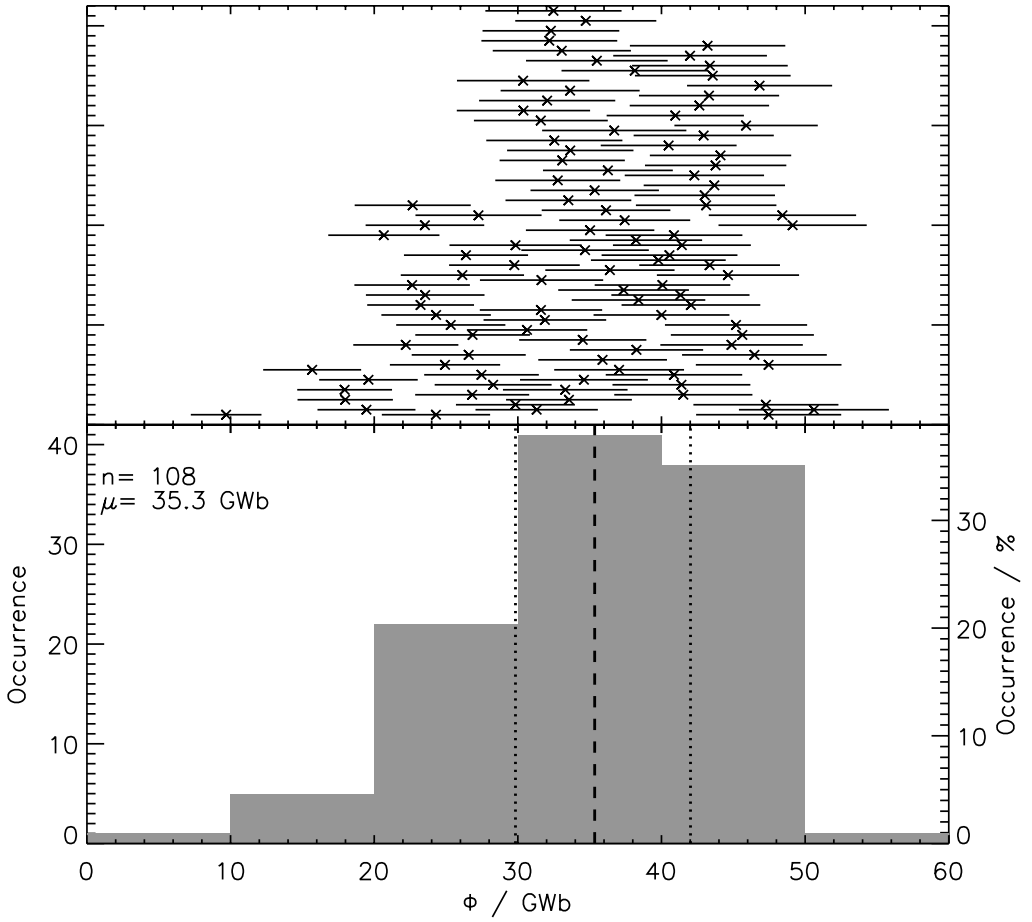

Figure 5: Distribution of estimated open flux, Φ, in 10 GWb bins. The lower panel shows a histogram of the values across bins of width 10 GWb, while the upper panel shows each value and its error bar. The distribution of values in the y-direction on the upper panel is simply to space the values so each error bar can be seen. The black dashed line on the lower panel marks the median of the distribution, and the two dotted lines mark the first and third quartiles.

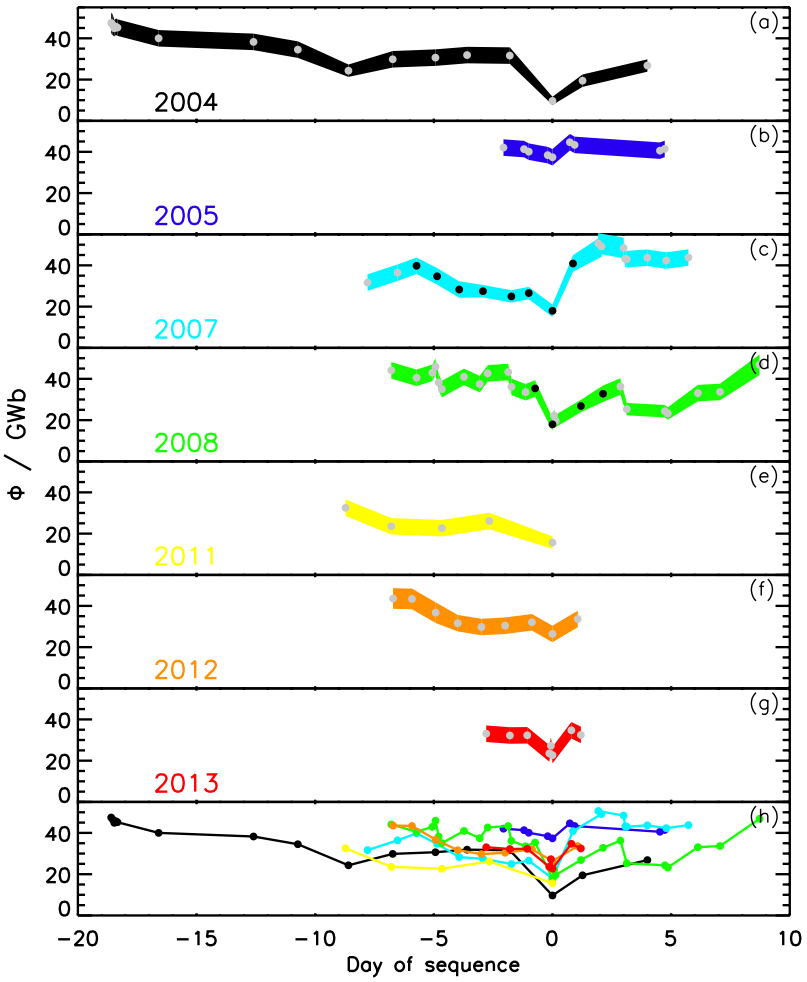

Figure 6: (a)–(f) Time series of open flux estimates for sequences of images in years 2004–2013. The coloured shading gives the uncertainty range on each estimate. Black dots indicate estimates obtained from images shown in Figures 2–3. Each time series is referenced to the time of the minimum open flux estimate in that sequence. (g) Open flux estimates for all campaigns from panels above.

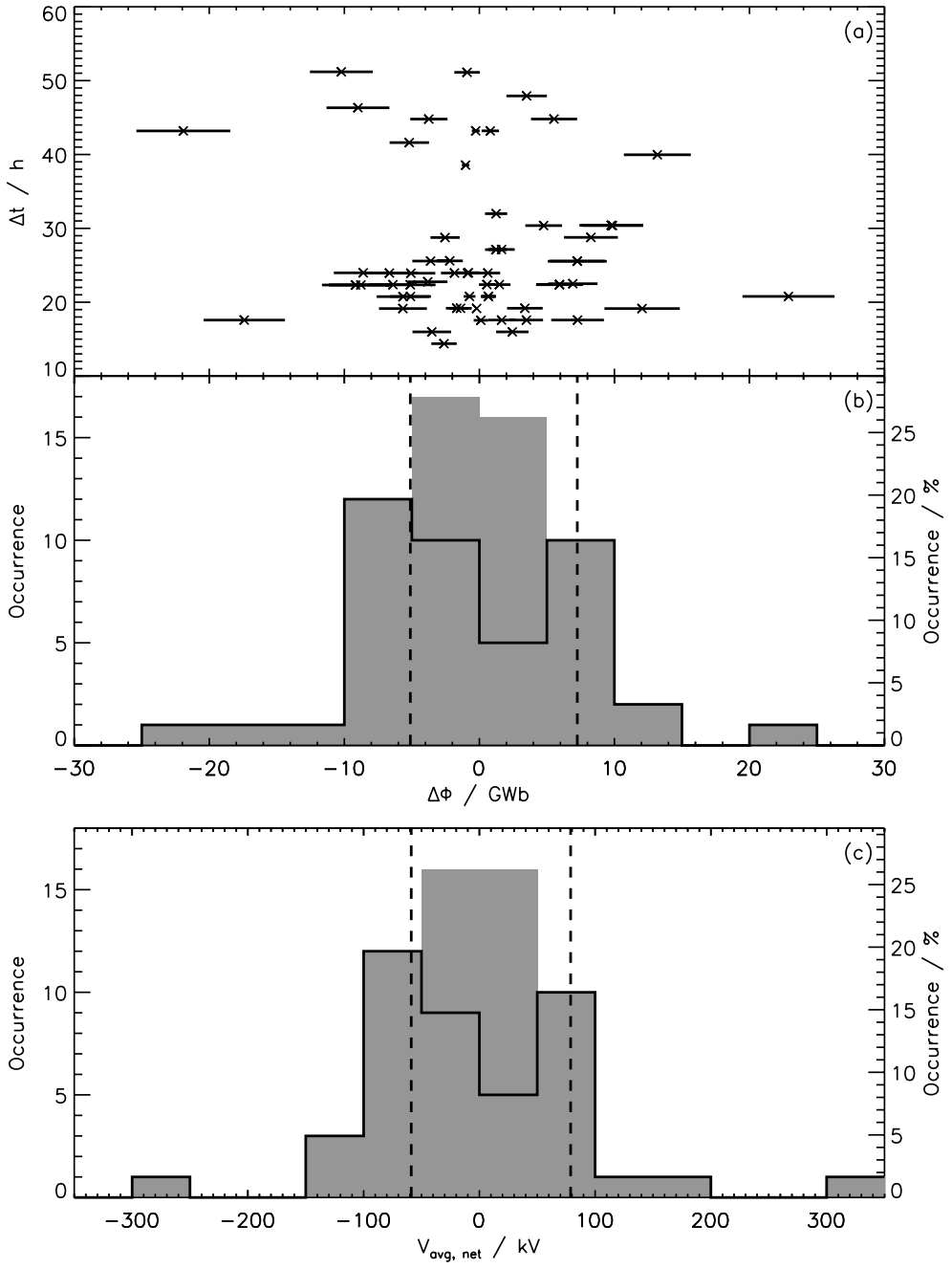

Figure 7: Changes in open flux, $\Delta\Phi$, and the derived average, net reconnection rates, $V_{avg,net}$. (a) $\Delta\Phi$ versus the time between images, Δt. (b) Distribution of $\Delta\Phi$ values. The grey shaded distribution represents all the values estimated, while the solid line represents the distribution of only those values of $\Delta\Phi$ larger than their associated errors. The vertical dashed lines show the median positive and negative values for the reduced distribution. (c) Distribution of $V_{avg,net}$ values in a similar format as (b).

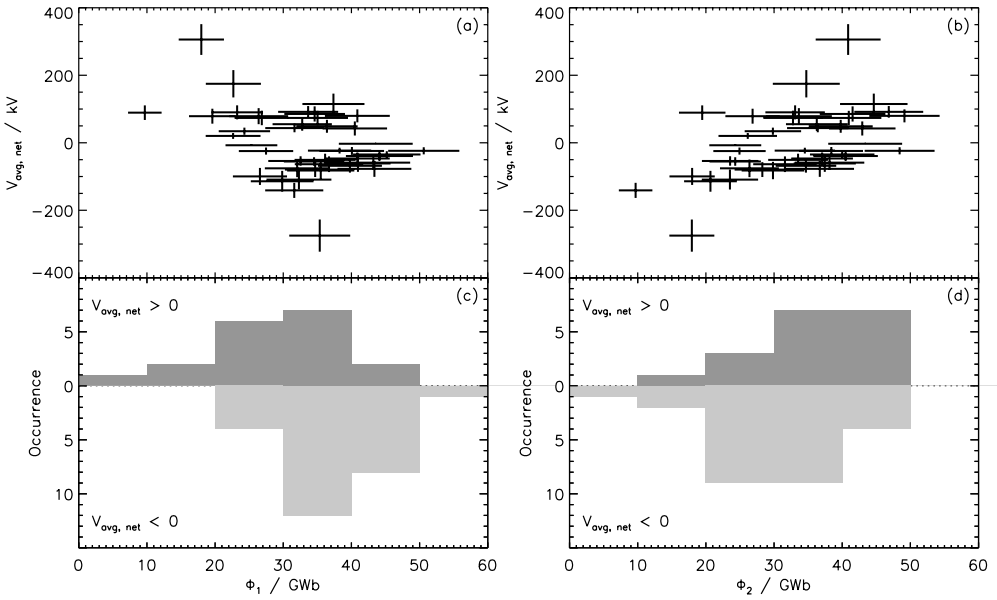

Figure 8: Average reconnection rates associated with each pair of successive open flux measurements Φ_1 and Φ_2. (a) Initial open flux, Φ_1, and $V_{avg,net}$ values and associated uncertainties. (b) Final open flux, Φ_2, and $V_{avg,net}$ and associated uncertainties. (c) The number of positive (upper, dark grey) and negative (lower, light grey) $V_{avg,net}$ values in each 10 GWb bin of Φ_1. (d) The same as (c) but for Φ_2.